Atractylenolide I inhibits the growth, proliferation and migration of B16 melanoma cells via the PI3K/AKT/mTOR pathway

XIAOCHUN XU, PING KANG and HONG CHE

Department of Dermatology, Ordos Central Hospital, Ordos, Inner Mongolia Autonomous Region 017010, P.R. China

Received September 19, 2024; Accepted March 24, 2025

DOI: 10.3892/ol.2025.15118

Abstract. Melanoma is a malignancy that affects millions of individuals worldwide. Atractylenolide I (AT) has been reported to suppress cell proliferation in melanoma cells, but the underlying mechanism is not fully understood. Therefore, the present study investigated the mechanism underlying the antitumor activity of AT in melanoma. Cell Counting Kit-8 and colony formation assays were performed after B16 and A875 melanoma cells were treated with 25, 50 and 100 μM AT. The results indicated that AT could significantly and dose-dependently suppress melanoma cell viability and proliferation ($P<0.001$). Furthermore, the stemness and migration of melanoma cells were significantly inhibited by the three doses of AT ($P<0.001$), as demonstrated by sphere formation and wound healing assays. Gene Ontology, Kyoto Encyclopedia of Genes and Genomes and target-pathway networks analyses identified the phosphatidylinositol 3-kinase/protein kinase B/mammalian target of rapamycin (PI3K/AKT/mTOR) axis as a potential target of AT in melanoma. Mechanistically, the suppression of viability, proliferation, stemness and migration by AT was significantly reversed by overexpression of PI3K in melanoma cells. However, AT did not affect melanoma cells when PI3K was knocked down, suggesting that the anti-melanoma effects of AT are mediated by PI3K. Additionally, the expression of phosphorylated (p-)PI3K, PI3K, p-AKT (Ser^{473}), p-AKT (Thr^{308}), AKT, p-mTOR (Ser^{2448}), p-mTOR (Ser^{2481}) and mTOR, determined via western blotting, revealed that the phosphorylation of PI3K, AKT and mTOR was significantly suppressed following AT treatment ($P<0.001$), further supporting the notion that AT exerts its antitumor activity through the PI3K/AKT/mTOR axis. In conclusion, the present study demonstrated that AT could inhibit the viability, proliferation and migration of melanoma cells through the PI3K/AKT/mTOR axis. These findings reveal a novel anti-melanoma effect and the therapeutic potential of AT in melanoma.

Correspondence to: Dr Xiaochun Xu, Department of Dermatology, Ordos Central Hospital, 6 Sudu Street, Kangbashi, Ordos, Inner Mongolia Autonomous Region 017010, P.R. China
E-mail: pfkxxc8593209@163.com

Key words: atractylenolide I, melanoma, network pharmacology, phosphatidylinositol 3-kinase/serine-threonine kinase/mammalian target of rapamycin

Introduction

Melanoma is characterized by the malignant transformation of melanocytes. This skin cancer is highly aggressive and drug-resistant, with a survival rate of only 29.8% after 5 years, and causes ~55,500 deaths annually (1,2). At present, the primary therapeutic strategy for melanoma involves surgical excision of the primary tumor followed by adjuvant treatment to prevent recurrence of the malignancy (3). First-line adjuvant treatments for melanoma include interferon-α and dabrafenib. However, these treatments have not been successful in markedly improving overall survival and often result in severe side effects (4-7). Therefore, the development of new adjuvants with high efficacy and low toxicity is required for the treatment of melanoma.

In recent years, Traditional Chinese Medicine (TCM) has gained increasing attention for its potential in the development of novel drugs for postoperative adjuvant treatment, due to its high efficacy and low toxicity (8-10). *Atractylodes macrocephala*, known as 'Baizhu' in Chinese, is a perennial herb with a history spanning thousands of years in treating various disorders, including spleen hypofunction, diarrhea and cancer (11,12). Both *in vitro* and *in vivo* experimental studies have demonstrated the antitumor activity of *A. macrocephala* rhizome extract (13-15). Atractylenolide I (AT) is a sesquiterpenoid lactone extracted from the *A. macrocephala* rhizome. AT induces apoptosis and suppresses glycolysis in colorectal cancer cells (16). The suppressive role of AT in tumorigenesis has also been reported in breast cancer (15). AT induces apoptosis and cell cycle arrest in melanoma cells via the extracellular regulated protein kinase/glycogen synthase kinase 3β axis (17). Additionally, Xu *et al* (18) discovered that AT enhances the responsiveness to immune checkpoint blockade therapy by activating tumor antigen presentation in colorectal cancer cell implanted C57BL/6 mice and human patient-derived colorectal cancer organoid models. Therefore, the promising therapeutic potential of AT in melanoma is supported by various studies. However, its precise role and underlying mechanisms remain largely unknown. Furthermore, the multitude of targets and complex interactions between AT and melanoma pose a major challenge in understanding the antitumor mechanism of action of AT.

Network pharmacology has recently emerged as a robust method for systematically revealing the biological mechanisms underlying complex diseases and natural ingredients in TCM (19,20). Unlike the traditional 'one symptom-one target-one drug' dogma, network pharmacology prefers to establish a 'compound-protein/gene-disease' synergistic network, sharing a similar holistic philosophy as that of TCM (21). This approach effectively provides an understanding of the mechanisms underlying complex interactions between diseases and TCM preparations, making it valuable for new drug discovery and, in particular, the modern analysis of TCM treatments. For example, *Ganoderma lucidum*, known as 'Ling Zhi' in China, is a typical TCM with anticancer properties, whose mechanism of action was analyzed using network pharmacology and experimental data (22). Additionally, Li *et al* (23) utilized network pharmacology to predict the immunoregulatory mechanisms of ginseng leaves in lung cancer. These findings indicate the potential value of network pharmacology as a strategy for enhancing the understanding of the underlying mechanisms of TCM in disease treatment.

Considering the complex interactions between AT and melanoma cells, to the best of our knowledge, the present study was the first to utilize network pharmacology and integrate experimental verification to uncover the underlying therapeutic mechanisms of AT in treating melanoma.

Materials and methods

Cell culture. B16 cells were obtained from Procell Life Science & Technology Co., Ltd. and A875 cells were acquired from the American Type Culture Collection. Both cell types were cultured in RPMI 1640 medium (MilliporeSigma), supplemented with penicillin/streptomycin (Corning, Inc.) and 10% fetal bovine serum (Gibco; Thermo Fisher Scientific, Inc.), at 37˚C in a humidified atmosphere with 5% CO_2.

Cell viability assay. B16 and A875 cells in the logarithmic phase were trypsinized, counted and seeded in 96-well plates at a density of $5x10^3$ cells/well in RPMI 1640 medium containing 10% fetal bovine serum. To investigate the cytotoxicity of AT (purity >98%; Chengdu Push Bio-Technology Co., Ltd.) in B16 cells and A875 cells, cells were cultured in media only (control), AT at 25 μM (AT-low group; AT-L), 50 μM (AT-medium group; AT-M) and 100 μM (AT-high group; AT-H) were added to the experimental wells for 24 h at 37˚C. After treatment, the original medium was replaced with 100 μl fresh medium containing 10 μl Cell Counting Kit-8 (CCK-8) reagent (cat. no. C0043; Beyotime Institute of Biotechnology). Optical density was measured at 450 nm using a microplate reader (Bio-Rad Laboratories, Inc.) to calculate the cell viability after a 2 h incubation with CCK-8 in a humidified incubator with 5% CO_2 at 37˚C. The assay was repeated thrice.

Colony formation assay. B16 and A875 cells were seeded in 6-well plates at a density of 2,000 cells/well (Corning, Inc.) and incubated for 10 days. The cells were then fixed with 4% paraformaldehyde for 30 min at room temperature, stained with crystal violet (Beijing Solarbio Science & Technology Co., Ltd.) at 25˚C for 30 min and washed thrice with 1X phosphate buffered saline. A cell population containing >50 cells (24) was considered a single colony. The number of colonies was counted using a light microscope (Leica Microsystems GmbH) and evaluated by ImageJ software (version 1.52m; National Institutes of Health,) using the ColonyArea plugin (https://imagej.net/plugins/colonyarea). The assay was performed in parallel using three biological replicates.

Sphere formation assay. To generate spheres, $4x10^3$ B16 and A875 cells, with or without AT treatment, were seeded in 24-well plates coated with 0.5 mg/ml poly-2-hydroxyethyl methacrylate ethanol solution (MilliporeSigma) to prevent cell attachment. To further promote the formation of sphere, cells were cultured in 1 ml RPMI 1640 supplemented with 20 ng/ml epidermal growth factor (Stemcell Technologies, Inc.), a 1:50 dilution of B27 supplement (Gibco; Thermo Fisher Scientific, Inc.) and 20 ng/ml recombinant human basic fibroblast growth factor (Promo Kine; PromoCell GmbH) and incubated in a humidified 5% CO_2 incubator at 37˚C for 7 days. Cell density was maintained at 4 cells/μl to prevent cell aggregation. Spheres (containing >50 cells) were counted through inverted light microscopy and data were evaluated by ImageJ and the ImageJ Bio-Formats Plugin (https://www.openmicroscopy.org/bio-formats/). The experiment was performed thrice to facilitate the statistical analysis of the data.

Wound healing assay. B16 and A875 cells were seeded into 6-well plates. Once the cells were at 90% confluency, the cell layer was disturbed using a sterile 200 μl pipette tip to generate a linear scratch wound on the cell surface. Subsequently, the cells were cultured in serum-free RPMI 1640 medium, with images collected at 0 and 24 h. Wound closure was assessed through a light microscopy and quantified using ImageJ software. The wound closure was calculated as the wound healing rate using the following formula: Wound healing rate (%)= (wound width at 0 h-wound width at 24 h)/wound width at 0 h x100%. The assay was performed independently three times in parallel.

AT target prediction. The Similarity Ensemble Approach (https://sea.bkslab.org/) and Swiss TargetPrediction (http://www.swisstargetprediction.ch/) databases were used to predict protein target for screening, with '*Homo sapiens*' specified as the restriction condition.

Melanoma target collection. Melanoma-related targets were sourced from various online medical databases, including GeneCards (https://www.genecards.org/) (25), DrugBank (https://go.drugbank.com/) (26), Online Mendelian Inheritance in Man (https://www.omim.org/) (27) and Therapeutic Target Database (https://db.idrblab.net/ttd/) (28). After obtaining melanoma-related disease targets, duplicates were removed and a database of disease-target information was created. Subsequently, melanoma disease targets were compared with AT therapeutic targets to identify overlapping targets. The significance threshold was set at -log(p) ≥5.

Gene Ontology (GO) and Kyoto Encyclopedia of Genes and Genomes (KEGG) analyses. The data were obtained using the following restriction conditions: 'OFFICIAL-GENE-SYMBOL', 'P<0.05' and '*Homo sapiens*'. GO and KEGG

pathway enrichment analyses were conducted using the DAVID database (29,30). The results were ranked in descending order based on the degree of target enrichment. Subsequently, the top 10 processes and pathways were selected and visualized.

Construction of the target-pathway network. Intersecting targets between AT and melanoma as well as notable pathways predicted using the KEGG database (https://www.kegg.jp/) were imported into Cytoscape 3.7.0 (https://cytoscape.org/) to construct the component-target-pathway network of AT. The importance of AT and the targets was determined according to Degree ≥5 (31), which indicates the total number of routes related to a node by other nodes. Increasingly higher degree values indicate increasing importance.

RNA interference and overexpression. To knock down phosphatidylinositol 3-kinase (PI3K) expression, B16 cells were transfected with PI3K-specific small interfering RNAs (siRNAs; Qiagen, Inc.) using Lipofectamine RNAiMAX (Invitrogen; Thermo Fisher Scientific, Inc.), according to the manufacturer's instructions. AllStars negative control (NC) siRNA (Qiagen, Inc.) was used as the experimental control. The sequences of the specific genes used in the present study are as follows: PI3K (#1) sense strand, 5'-AGAAAACCGCCU UAUGGAGUC-3' and antisense strand, 5'-CUCCAUAAG GCGGUUUUCUAU-3'; PI3K (#2) sense strand, 5'-AUAGAA AACCGCCUUAUGGAG-3' and antisense strand, 5'-CCA UAAGGCGGUUUUCUAUGU-3'; siNC 5'-AATTCTCCG AACGTGTCACGT-3' and antisense strand, 5'-UUAAGA GGCTTGCACAGTGCA-3'. For PI3K overexpression in A875 cells, the cDNA encoding PI3K (NCBI reference sequence, NM_006218.4) was amplified via PCR and subcloned into the pcDNA3.1 vector (Invitrogen; Thermo Fisher Scientific, Inc.) to construct the PI3K overexpression (oe) vector, with an empty vector serving as a NC. B16 and A875 cells seeded in 6-well plates at a density of $1x10^6$ cells/well were transfected with the aforementioned siRNAs or vectors (PI3K-specific siRNAs and siNC, 50 nM; PI3K oe vector and empty vector, 2 μg) at 37˚C. The expression levels of PI3K in transfected cells were quantified using reverse transcription-quantitative polymerase chain reaction (RT-qPCR) and western blotting 48 h post-transfection.

RT-qPCR. Total RNA was isolated from B16 cells and A875 using TRIzol reagent according to the manufacturer's instructions (Invitrogen; Thermo Fisher Scientific, Inc.). Reverse Transcription was performed with the GoScript™ Reverse Transcription kit (Promega Corporation) according to the manufacturer's instructions. Briefly, 500 ng of total RNA was reverse transcribed in a 20 μl reaction volume using oligo(dT) primers and M-MLV reverse transcriptase. The reaction was incubated at 42˚C for 60 min, followed by enzyme inactivation at 70˚C for 15 min. qPCR was subsequently performed on the LightCycler System 2.0 (Roche Diagnostics GmbH) with the following thermocycling conditions: Initial pre-denaturation for 2 min at 90˚C, followed by 40 cycles at 93˚C for 10 sec, 60˚C for 15 sec and 72˚C for 15 sec. Evaluation of the solubility curve was performed at 95˚C for 5 sec and 60˚C for 1 min, followed by cooling at 42˚C for 30 sec. The primer sequences for PI3K and β-actin are listed in Table SI. The expression level of each gene was analyzed using a SYBR Green kit (Promega Corporation). Relative quantitation analysis was conducted based on the $2^{-\Delta\Delta Cq}$ method (32), with β-actin serving as the internal control. The RT-qPCR assays were conducted in triplicate.

Western blotting. Briefly, RIPA buffer (Beyotime Institute of Biotechnology) containing a protease inhibitor cocktail (Roche Diagnostics GmbH) was used to extract proteins from the cells. Protein concentrations were determined using a BCA kit (Beyotime Institute of Biotechnology). Next, all protein samples (20 μg per lane) were separated using 8% sodium dodecyl-sulfate polyacrylamide gel electrophoresis and transferred to polyvinylidene difluoride membranes. Different membranes were used for probing phosphorylated and non-phosphorylated proteins to ensure optimal blocking and detection conditions. The membranes were blocked for 2 h at 25˚C using 8% skim milk for β-actin as well as non-phosphorylated proteins, and 5% bovine serum albumin (Gibco; Thermo Fisher Scientific, Inc.) for the phosphorylated proteins. The membranes were then incubated with the corresponding primary antibodies at 4˚C overnight, followed by incubation with secondary antibodies for 1 h at 25˚C. Finally, the ECL Kit (cat. no. ab65623; Abcam) was used to visualize the protein bands through an ECL imaging system (Tanon Science and Technology Co., Ltd.). Band intensity was semi-quantified using ImageJ. The following antibodies were provided by Beyotime Institute of Biotechnology: PI3K antibody (cat. no. AF7749; 1:1,000), Phosphorylated (p)-PI3K (cat. no. AF5905; 1:1,000), protein kinase B (AKT; cat. no. AA326; 1:1,000), p-AKT (Ser^{473}; cat. no. AA329; 1:1,000), p-AKT (Thr^{308}; cat. no. AA331; 1:1,000), mammalian target of rapamycin (mTOR; cat. no. AF1648; 1:1,000), p-mTOR (Ser^{2448}; cat. no. AF5869; 1:1,000) and β-actin (cat. no. AF0003; 1:2,000). p-mTOR antibody (Ser^{2481}; cat. no. abs130934; 1:1,000) was purchased from Absin Bioscience, Inc. The HRP-conjugated secondary antibodies were purchased from Abcam (cat. nos. ab6721 and ab6728; 1:2,000). All western blotting experiments were repeated thrice.

Statistical analysis. GraphPad Prism (version 8.0.2; Dotmatics) was used for the data analyses. All data are presented as the mean ± standard error of the mean. The normality of the data was tested using the Shapiro-Wilk test, with $P<0.05$ considered to indicate normally distributed data. Homogeneity of variance was tested using Levene's test, with $P>0.05$ considered to indicate homogenous data. For data that met normal distribution assumptions and equal variances, statistical analyses were performed through one-way analysis of variance and Bonferroni post hoc test for multiple comparisons. Two-way ANOVA followed by Bonferroni post hoc test was used for experiments involving multiple independent variables (such as time and dose-dependent comparisons of the cytotoxicity of AT). $P<0.05$ was considered to indicate a statistically significant difference.

Results

AT inhibits the proliferation, stemness and migration of melanoma cells. The chemical structure of AT is shown in

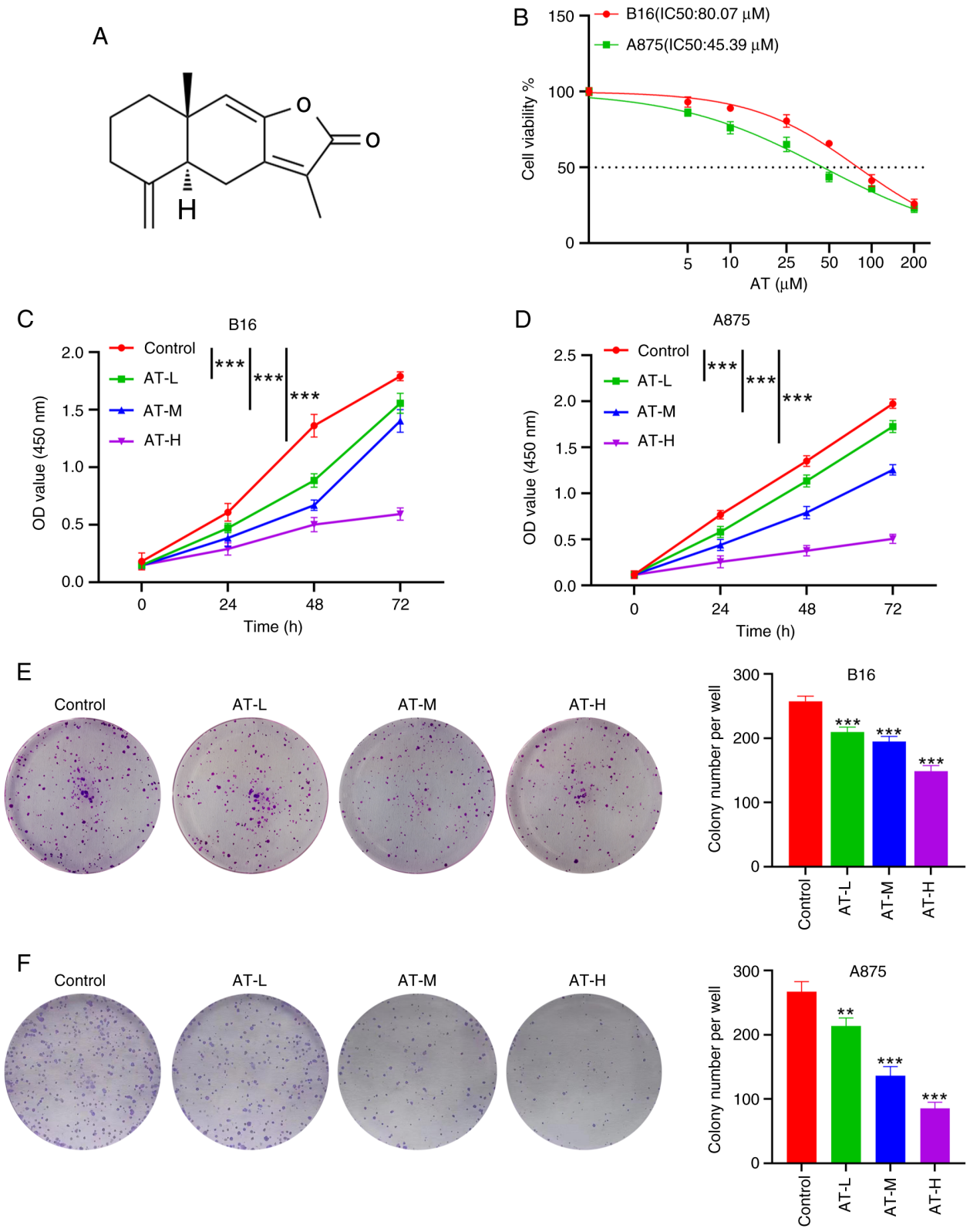

Figure 1. AT inhibits the proliferation, stemness and migration of melanoma cells. (A) The chemical structure of AT. (B) The IC_{50} values of AT in B16 and A875 cells were calculated based on cell viability after the cells were treated with a series of concentrations of AT. OD values of (C) B16 and (D) A875 cells from different groups following incubation with Cell Counting Kit-8. Proliferation capacity of (E) B16 and (F) A875 cells quantified via the colony formation assay. **P<0.01, ***P<0.001 vs. the Control group. AT, atractylenolide I; IC_{50}, half-maximal inhibitory concentration; OD, optical density; AT-L, AT-low; AT-M, AT-medium; AT-H, AT-high.

Fig. 1A. To evaluate the antitumor activity of AT, B16 and A875 melanoma cells were initially co-cultured with a series of concentrations of AT (5, 10, 25, 50, 100 and 200 μM) for 24 h to calculate the half-maximal inhibitory concentration (IC_{50}) of AT. The AT IC_{50} values were 80.07 μM for B16 cells and 45.39 μM for A875 cells (Fig. 1B). Next, doses of 25 μM (AT-L),

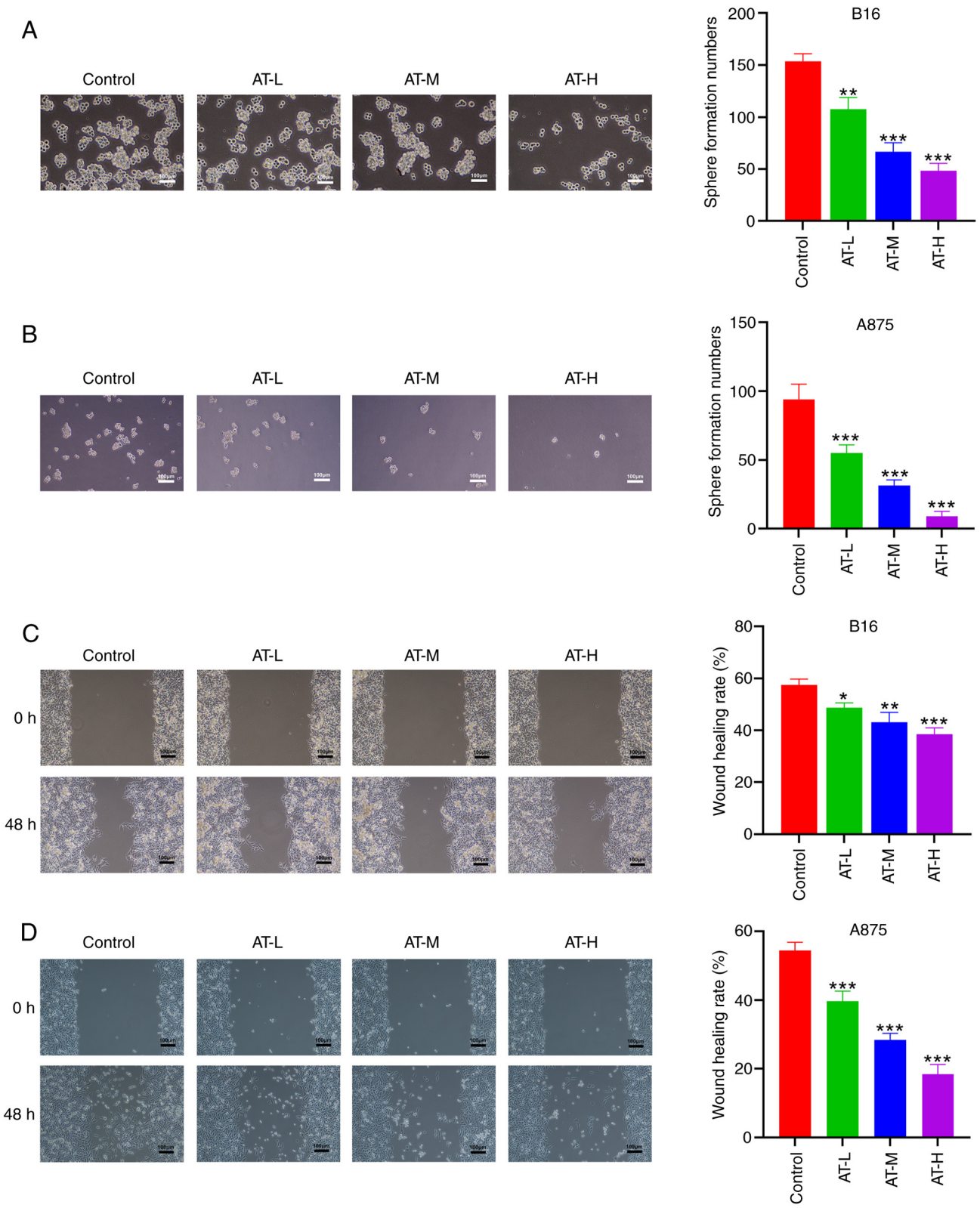

Figure 2. AT suppresses the stemness and migration of melanoma cells. Stemness of (A) B16 and (B) A875 cells were assessed by sphere formation assay. Migration ability of (C) B16 and (D) A875 cells were analyzed via wound healing assay. *P<0.05, **P<0.01, ***P<0.001 vs. the Control group. AT, atractylenolide I; IC_{50}, half-maximal inhibitory concentration; AT-L, AT-low; AT-M, AT-medium; AT-H, AT-high.

50 μM (AT-M) and 100 μM (AT-H) were chosen to explore the cytotoxicity of AT in melanoma cells. After 24, 48 and 72 h of treatment, the viability of B16 cells was significantly reduced by all three AT doses in both a time-dependent (P<0.001) and dose-dependent (P<0.001) manner, as revealed by the CCK-8 assay (Fig. 1C). Similar findings were observed in A875 cells (both P<0.001; Fig. 1D), supporting the antitumor effect of AT on melanoma cells. Additionally, a colony formation

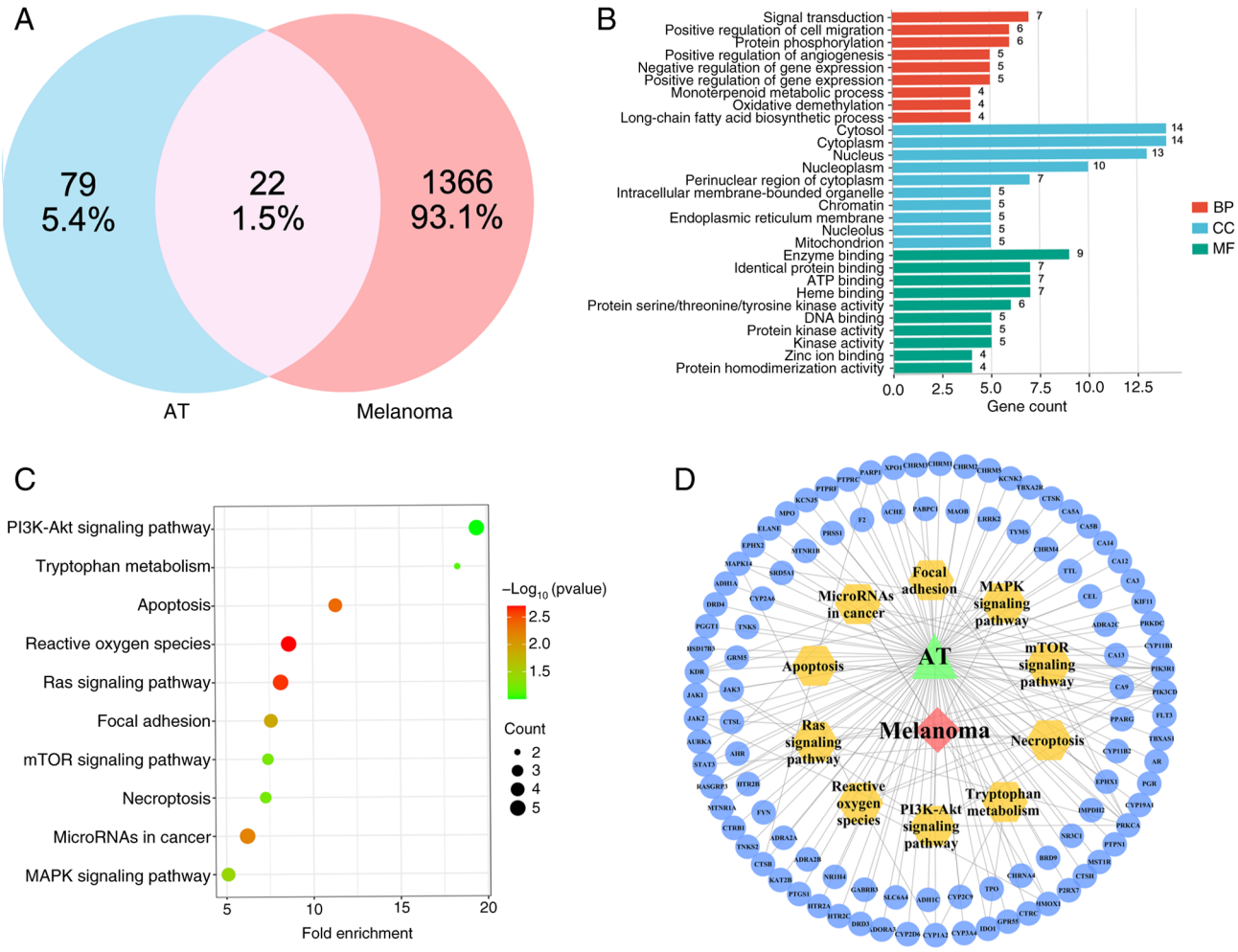

Figure 3. Prediction of the mechanism underlying the therapeutic effects of AT via network pharmacology. (A) Venn diagram of AT-melanoma intersection targets. Intersection targets investigated via (B) Gene Ontology and (C) Kyoto Encyclopedia of Genes and Genomes analyses. (D) The underlying therapeutic action of AT against melanoma shown in the target-pathway network. The blue dots represent intersection targets, yellow hexagons represent important pathways and edges represent the relationships among targets, pathways and specific objects (AT or melanoma). AT, atractylenolide I; BP, biological process; CC, cellular component; MF, molecular function.

assay was performed to evaluate the antiproliferative effect of AT on melanoma cells. Compared with the colony numbers in the control group, the number of melanoma cell colonies in the AT-L, AT-M and AT-H groups were significantly reduced (Fig. 1E and F). Collectively, these results indicate a suppressive role for AT in melanoma proliferation.

Since cancer stemness plays a crucial role in the recurrence and metastasis of malignancy (33), the suppressive effect of AT on the stemness of melanoma cells was examined using a sphere formation assay. The results indicated a significant decrease in the number of spheres formed by the B16 and A875 cells after AT treatment (Fig. 2A and B). The collective results suggest that AT could inhibit the stemness of melanoma cells. Additionally, as shown in Fig. 2C and D, the migration of both B16 and A875 cells was also significantly hindered by AT treatment. The collective data indicate that AT effectively inhibits the proliferation, stemness and migration of melanoma cells in a dose-dependent manner.

Prediction of the mechanism of action of AT via network pharmacology. After confirming the antitumor effects of AT, its mechanism of action was the next focus. However, the therapeutic targets and interactions between AT and melanoma are complex, making it difficult to determine the most likely therapeutic pathway. Network pharmacology was used to predict the main axis and reveal the potential therapeutic mechanisms of AT in melanoma. A total of 22 overlapping target genes were identified from the 79 AT and 1,366 melanoma target genes (Fig. 3A). Subsequently, all intersecting target genes were subjected to GO and KEGG enrichment analyses using the DAVID database. The results revealed that 105 biological processes, 16 related cellular components and 78 molecular functions were involved in the interactions between AT and melanoma. The pathways associated with the top 10 intersecting targets were considered for the construction of a GO enrichment analysis pathway map (Fig. 3B).

KEGG enrichment analysis was used to determine the signaling pathways associated with the anti-melanoma effects of AT. KEGG enrichment analysis yielded 62 statistically significant pathways, and the top ten KEGG enrichment analyses are shown in Fig. 3C. Among these, the 'PI3K-Akt signaling pathway' stood out as a potential axis in AT treatment, with a high -$\log_{10}$(P-value) of 9.99x10^{-2} and a gene count of 5. Since the

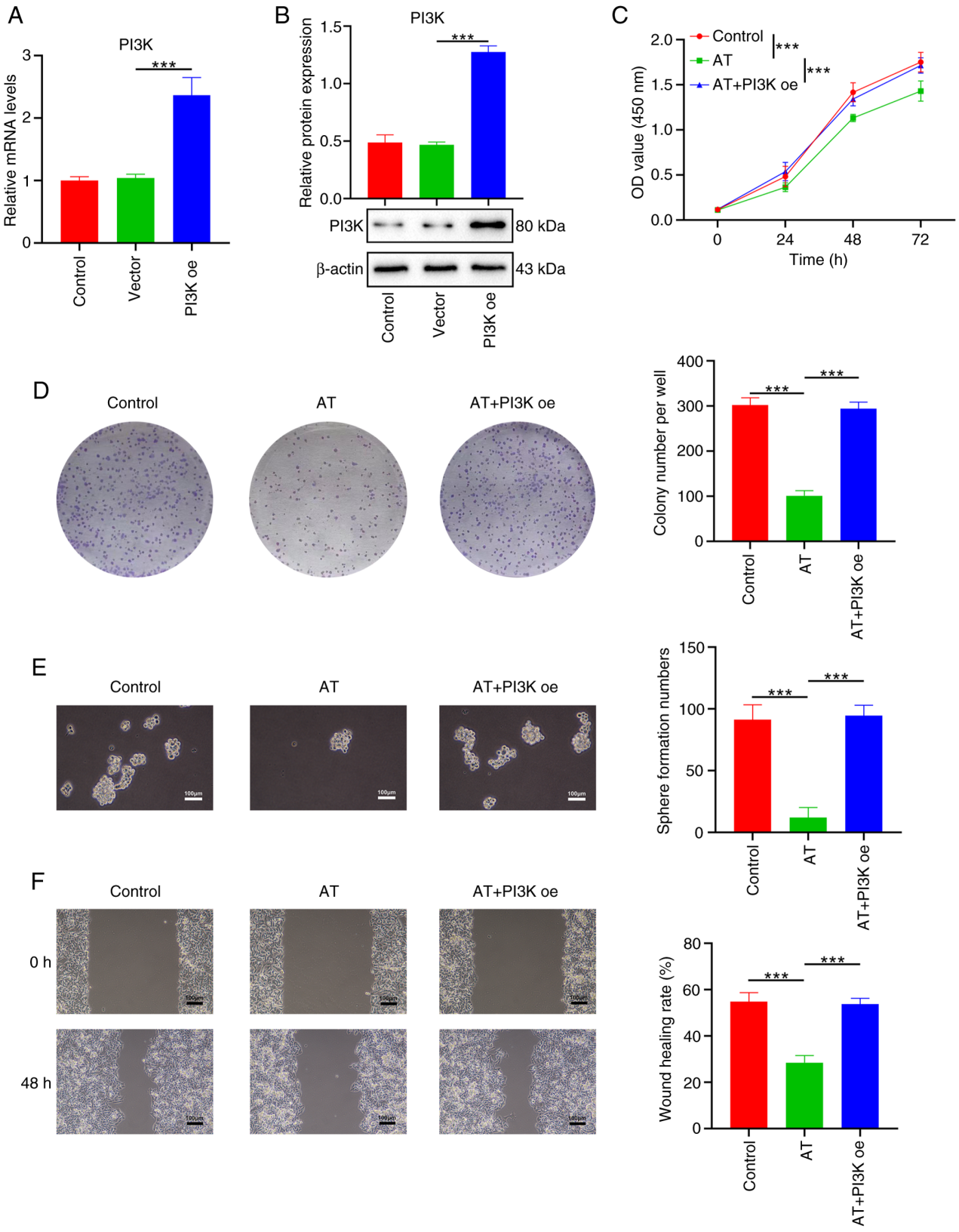

Figure 4. Overexpression of PI3K reverses the suppressive effects of AT in melanoma cells. PI3K overexpression efficiency was verified via (A) PCR and (B) western blotting. (C) OD of B16 cells following incubation with Cell Counting Kit-8. Proliferation ability, stemness and migration capacity of B16 cells was measured via (D) colony formation assay, (E) sphere formation assay and (F) wound healing assay, respectively. ***P<0.001. AT, atractylenolide I; PI3K, phosphatidylinositol 3-kinase; PI3K oe, PI3K overexpression vector. OD, optical density;

mTOR signaling pathway is a well-known downstream pathway of the PI3K/AKT signaling pathway, the PI3K/AKT/mTOR axis was chosen for further exploration of the therapeutic mechanism of AT. Additionally, the PI3K/AKT and mTOR signaling pathways were selected as crucial pathways due to their high degree values (8 for the PI3K/AKT axis and 5 for the mTOR axis) in

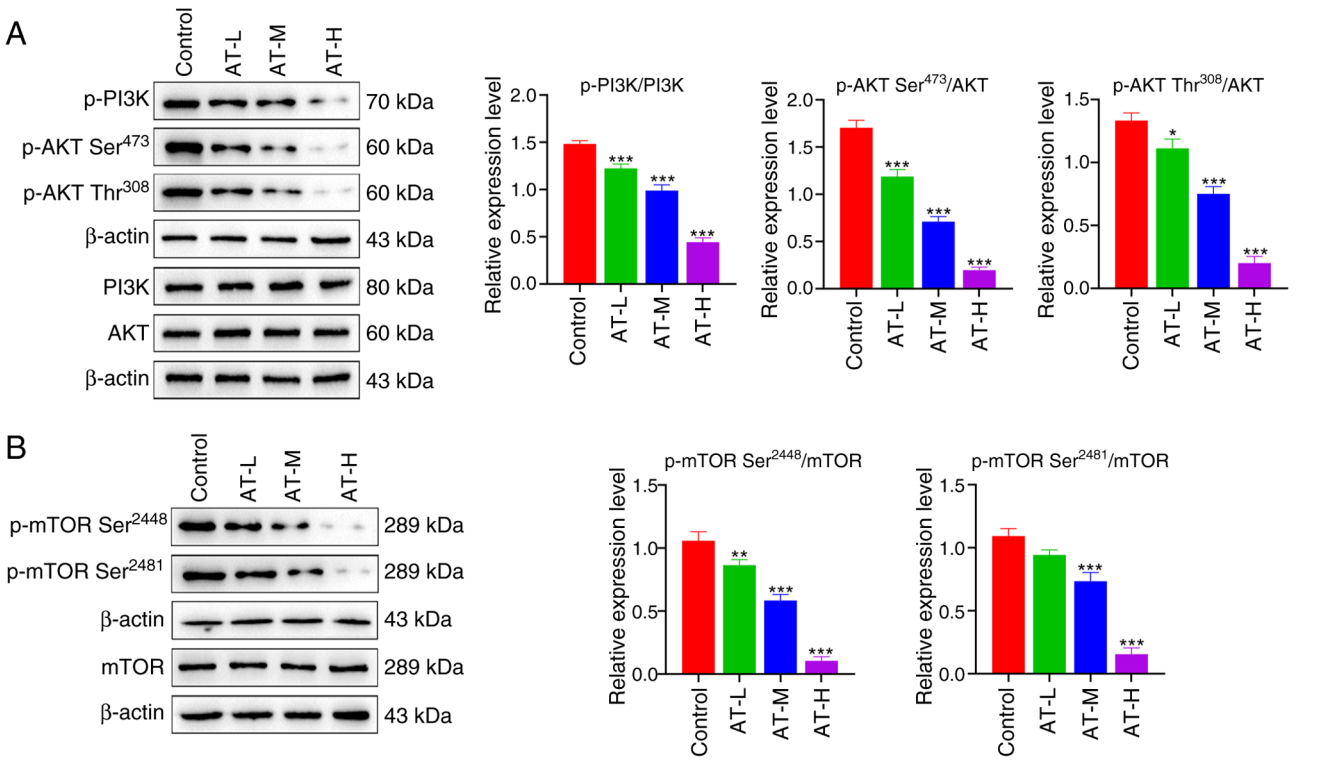

Figure 5. AT inhibits the PI3K/AKT/mTOR pathway in melanoma cells. (A) Expression levels of p-PI3K, PI3K, p-AKT (Ser^{473}), p-AKT (Thr^{308}) and AKT were measured via western blotting. (B) Expression levels of p-mTOR (Ser^{2448}), p-mTOR (Ser^{2481}) and mTOR were measured via western blotting. $^{*}P<0.05$, $^{**}P<0.01$, $^{***}P<0.001$ vs. the control group. AT, atractylenolide I; AT-L, AT-low; AT-M, AT-medium; AT-H, AT-high; p-, phosphorylated; PI3K, phosphatidylinositol 3-kinase; AKT, protein kinase B; mTOR, mammalian target of rapamycin.

the target-pathway network (Fig. 3D). Therefore, based on the network pharmacology results, it is reasonable to consider the PI3K/AKT/mTOR axis as the mechanism underlying the therapeutic effects of AT in melanoma.

Overexpression of PI3K reverses the suppressive effects of AT in melanoma cells. The role of PI3K in the suppressive effects of AT on melanoma cells was explored. Transfection of the PI3K oe vector successfully overexpressed PI3K in A875 cells, as demonstrated by RT-qPCR (Fig. 4A) and western blotting (Fig. 4B). Consistently, AT treatment significantly suppressed the cell viability, proliferation, stemness as well as migration of B16 cells (Fig. 4C-F), while the effects of AT were reversed by overexpressing PI3K (Fig. 4C-F).

To confirm the contribution of the PI3K/AKT/mTOR pathway to the effects AT of observed, the effects after PI3K knockdown were studied. The efficiency of PI3K knockdown was measured at both the RNA and protein levels, and siPI3K#2 was selected for subsequent experiments based on the results (Fig. S1A and B). As expected, the cell viability, proliferation, stemness and migration of B16 cells were significantly reduced after knocking down PI3K expression, which indicated that PI3K contributes to the malignant phenotypes of B16 cells. Additionally, in the absence of PI3K, AT did not significantly affect the cell viability, proliferation, stemness and migration of B16 cells, supporting the hypothesis that the inhibitory effect of AT on melanoma cells relies on its regulation of PI3K (Fig. S1C-F). In summary, PI3K signaling was demonstrated to be a major axis through which AT inhibits the viability, proliferation, stemness and migration of melanoma cells.

AT inhibits the PI3K/AKT/mTOR pathway in melanoma cells. After determining the role of PI3K signaling in AT activity, the effect of AT on the expression of the PI3K/AKT/mTOR axis in B16 cells was investigated. As shown in Fig. 5A, AT treatment significantly decreased the phosphorylation of PI3K and AKT. As a downstream target of the PI3K/AKT axis, mTOR signaling has been widely reported to promote proliferation in various cancer types (34). In the present study, the phosphorylation of mTOR was significantly suppressed by AT treatment, as shown in Fig. 5B. These results further imply that the inhibition of the PI3K/AKT/mTOR axis may be an underlying mechanism of action of AT in melanoma treatment.

Discussion

AT has been used to treat splenic and stomach ailments in Asia for centuries (35,36). Previous pharmacological studies have reported various activities of AT, such as antioxidant, anti-inflammatory and anticancer activities (37-39). Melanoma is one of the most common skin carcinomas worldwide and affects millions of individuals annually (40). The results of the present study demonstrated that AT effectively inhibited the growth and proliferation of melanoma cells, underscoring its potential for melanoma treatment.

Since malignant metastasis always occurs in patients with advanced melanoma and poses a major challenge to clinical therapy (41), the suppressive effect of AT on the migration of melanoma cells was investigated in the present study. AT treatment significantly inhibited cell migration, suggesting the potential of AT as an adjuvant treatment to prevent

melanoma metastasis. Similar to these results, Fu *et al* (42) demonstrated that AT inhibits the migration of melanoma cells and suggested that the role of AT may be mediated by the Janus kinase 2 (JAK2)/signal transducer and activator of transcription 3 (STAT3) pathway. However, the bioinformatics analysis performed in the present study suggested the potential role of the PI3K/AKT signaling pathway in AT activity during melanoma treatment and the JAK2/STAT3 pathway was not revealed in the analysis. Hence, the JAK2/STAT3 pathway was not explored further in the present study. Metastatic progression is affected by various factors, including post-transcriptional regulation, cancer stemness and epithelial-mesenchymal transition (EMT). Among these, stemness has been shown to play a role in AT treatment of melanoma metastasis (43). Cancer stemness is often characterized by the ability of specific cancer cells to self-renew, differentiate and regenerate. The induction of stemness in cancer cells is closely related to the proliferation, migration and drug resistance of melanoma cells (44,45). In the present study, AT treatment significantly inhibited the stemness of B16 cells, which may be a key factor in the therapeutic effect of AT on melanoma metastasis. EMT is a process characterized by the loss of epithelial cell markers and upregulation of mesenchymal cell markers. This process is another critical factor in cancer cell metastasis (46). Li *et al* (47) showed that fibronectin 1 promotes melanoma proliferation and metastasis through apoptosis and EMT. Additionally, evidence suggests a positive crosstalk between stemness and EMT in cancer cells (48), with EMT transcription factors playing a role in regulating tumor cell stemness (49). Notably, a previous study demonstrated the suppression of EMT by AT in prostate cancer cells (50). Considering the marked inhibitory effect of AT on the stemness of melanoma cells, EMT may also be suppressed by AT treatment.

Although the inhibitory effect of AT on cancer progression has been demonstrated, its specific mechanisms of action remain unknown. In the present study, the mechanism underlying the anti-melanoma effects of AT was investigated using network pharmacology. Based on these data, the PI3K/AKT signaling pathway was considered the key pathway for AT activity, whereas mTOR was identified as a notable downstream effector of the PI3K axis. The crucial role of PI3K/AKT signaling in melanoma pathophysiology has been emphasized by network pharmacology and extensive preliminary research (51,52). Inhibiting the PI3K/AKT/mTOR axis sensitizes melanoma cells to cisplatin and temozolomide (53). Previous studies on other diseases have demonstrated a relationship between AT and the PI3K/AKT/mTOR pathway. For example, AT effectively inhibits colorectal tumor progression both *in vitro* and *in vivo*, mainly by regulating the AKT/mTOR signaling pathway (14). In addition, the antitumor effect of AT in bladder cancer cells reportedly relies on the inhibition of the PI3K/Akt/mTOR signaling pathway (54). Moreover, Wang *et al* (55) recently demonstrated that AT suppresses the osteogenic differentiation of human valve interstitial cells by regulating the PI3K/AKT pathway. Similarly, the present study confirmed that this axis is essential for AT activity in melanoma cells, as revealed by PI3K knockdown and overexpression experiments.

PI3K is an intracellular phosphatidylinositol kinase that regulates cell survival, growth, proliferation, angiogenesis and metabolism in human cancer via the PI3K/AKT/mTOR pathway (56,57). In the present study, the phosphorylation of PI3K and AKT in B16 cells was significantly inhibited by AT treatment, suggesting that AT inhibits melanoma cells through the PI3K signaling pathway. AT has been shown to effectively inhibit the migration of B16 cells and the phosphorylation of AKT (58), which is consistent with the results of the present study. Following activation, AKT promotes the phosphorylation of tuberous sclerosis complex 2, which then activates the mammalian target of rapamycin complex 1 (mTORC1). AKT directly activates mTORC1 by phosphorylating Ser2448 (59). In the present study, mTOR phosphorylation at different sites (Ser 2448 and Ser2481) was significantly downregulated by AT treatment.

Taken together, the results of the present study confirm the anti-melanoma effects of AT. Additionally, the PI3K/AKT/mTOR axis was identified as an underlying mechanism of action of AT, as revealed by network pharmacology predictions and experimental validation. The significant suppressive effect of AT on melanoma suggests its potential as a novel drug for melanoma treatment. AT has several advantages that may facilitate its future use. First, clinical evidence suggests that AT is safe and exhibits low toxicity without serious adverse reactions (60). Second, a previous study reported that AT sensitizes human ovarian cancer cells to paclitaxel, indicating that the combination of AT with current chemotherapies may overcome drug resistance (61). Thus, AT is a valuable natural component that may play a role in the treatment of *melanoma*, either individually or in combination with other chemotherapeutic agents.

However, the present study has some limitations. Since all experiments were conducted *in vitro*, robust animal models are needed to verify the anti-melanoma properties and underlying mechanisms of action of AT. The PI3K family consists of three classes of phosphatidylinositol kinases (I/II/III); therefore, the regulatory role of AT should be thoroughly explored by further investigating which phosphatidylinositol kinases AT interacts with. Although the suppressive effect of AT on PI3K expression has been confirmed, further investigation is required to understand the interaction between AT and PI3K. Further detailed research on the regulation of the PI3K/AKT/mTOR axis by AT is required.

In conclusion, the present study demonstrated the anti-melanoma activity of AT and identified the PI3K/AKT/mTOR axis as a key mechanism underlying its therapeutic action, as confirmed through network pharmacology and experimental validation.

Acknowledgements

Not applicable.

Funding

No funding was received.

Availability of data and materials

The data generated in the present study may be requested from the corresponding author.

Authors' contributions

XCX and PK designed the experiments. PK and HC performed the experiments and analyzed the results. PK and HC confirm the authenticity of all the raw data. XCX wrote and revised the manuscript. All authors read and approved the final version of the manuscript.

Ethics approval and consent to participate

Not applicable.

Patient consent for publication

Not applicable.

Competing interests

The authors declare that they have no competing interests.

References

1. Huang AC and Zappasodi R: A decade of checkpoint blockade immunotherapy in melanoma: Understanding the molecular basis for immune sensitivity and resistance. Nat Immunol 23: 660-670, 2022.
2. Schadendorf D, van Akkooi ACJ, Berking C, Griewank KG, Gutzmer R, Hauschild A, Stang A, Roesch A and Ugurel S: Melanoma. Lancet 392: 971-984, 2018.
3. Eddy K and Chen S: Overcoming immune evasion in melanoma. Int J Mol Sci 21: 8984, 2020.
4. Rubin KM, Vona K, Madden K, McGettigan S and Braun IM: Side effects in melanoma patients receiving adjuvant interferon alfa-2b therapy: A nurse's perspective. Support Care Cancer 20: 1601-1611, 2012.
5. Hauschild A, Gogas H, Tarhini A, Middleton MR, Testori A, Dréno B and Kirkwood JM: Practical guidelines for the management of interferon-alpha-2b side effects in patients receiving adjuvant treatment for melanoma: Expert opinion. Cancer 112: 982-994, 2008.
6. Hersey P, Tiffen JC and Gallagher SJ: Shedding light on dabrafenib-induced fevers in patients with melanoma. Lancet Oncol 20: 1637-1638, 2019.
7. Sloot S, Fedorenko IV, Smalley KS and Gibney GT: Long-term effects of BRAF inhibitors in melanoma treatment: Friend or foe? Expert Opin Pharmacother 15: 589-592, 2014.
8. Liu X, Li M, Wang X, Dang Z, Yu L, Wang X, Jiang Y and Yang Z: Effects of adjuvant traditional Chinese medicine therapy on long-term survival in patients with hepatocellular carcinoma. Phytomedicine 62: 152930, 2019.
9. Wang R, Sun Q, Wang F, Liu Y, Li X, Chen T, Wu X, Tang H, Zhou M, Zhang S, *et al*: Efficacy and safety of Chinese herbal medicine on ovarian cancer after reduction surgery and adjuvant chemotherapy: A systematic review and meta-analysis. Front Oncol 9: 730, 2019.
10. Zhou Y, Wang M, Wang Z, Qiu J, Wang Y, Li J, Dong F, Huang X, Zhao J and Xu T: Polysaccharides from hawthorn fruit alleviate high-fat diet-induced NAFLD in mice by improving gut microbiota dysbiosis and hepatic metabolic disorder. Phytomedicine 139: 156458, 2025.
11. Hoang LS, Tran MH, Lee JS, Ngo QM, Woo MH and Min BS: Inflammatory inhibitory activity of sesquiterpenoids from atractylodes macrocephala Rhizomes. Chem Pharm Bull (Tokyo) 64: 507-511, 2016.
12. Shu YT, Kao KT and Weng CS: In vitro antibacterial and cytotoxic activities of plasma-modified polyethylene terephthalate nonwoven dressing with aqueous extract of Rhizome Atractylodes macrocephala. Mater Sci Eng C Mater Biol Appl 77: 606-612, 2017.
13. Kou N, Cho H, Kim HE, Sun Q, Ahn K, Ji H, Choi H and Kim O: Anti-cancer effect of Atractylodes macrocephala extract by double induction of apoptotic and autophagic cell death in head and neck cancer cells. Bangladesh J Pharmacol 12: 140-146, 2017.
14. Wang K, Huang W, Sang X, Wu X, Shan Q, Tang D, Xu X and Cao G: Atractylenolide I inhibits colorectal cancer cell proliferation by affecting metabolism and stemness via AKT/mTOR signaling. Phytomedicine 68: 153191, 2020.
15. Long F, Lin H, Zhang X, Zhang J, Xiao H and Wang T: Atractylenolide-I suppresses tumorigenesis of breast cancer by inhibiting toll-like receptor 4-mediated nuclear factor-κB signaling pathway. Front Pharmacol 11: 598939, 2020.
16. Li Y, Wang Y, Liu Z, Guo X, Miao Z and Ma S: Atractylenolide I induces apoptosis and suppresses glycolysis by blocking the JAK2/STAT3 signaling pathway in colorectal cancer cells. Front Pharmacol 11: 273, 2020.
17. Ye Y, Chao XJ, Wu JF, Cheng BC, Su T, Fu XQ, Li T, Guo H, Tse AK, Kwan HY, *et al*: ERK/GSK3β signaling is involved in atractylenolide I-induced apoptosis and cell cycle arrest in melanoma cells. Oncol Rep 34: 1543-1548, 2015.
18. Xu H, Van der Jeught K, Zhou Z, Zhang L, Yu T, Sun Y, Li Y, Wan C, So KM, Liu D, *et al*: Atractylenolide I enhances responsiveness to immune checkpoint blockade therapy by activating tumor antigen presentation. J Clin Invest 131: e146832, 2021.
19. Khanal P and Patil BM: Integration of network and experimental pharmacology to decipher the antidiabetic action of Duranta repens L. J Integr Med 19: 66-77, 2021.
20. Zeng P, Su HF, Ye CY, Qiu SW, Shi A, Wang JZ, Zhou XW and Tian Q: A tau pathogenesis-based network pharmacology approach for exploring the protections of Chuanxiong Rhizoma in Alzheimer's disease. Front Pharmacol 13: 877806, 2022.
21. Nogales C, Mamdouh ZM, List M, Kiel C, Casas AI and Schmidt H: Network pharmacology: Curing causal mechanisms instead of treating symptoms. Trends Pharmacol Sci 43: 136-150, 2022.
22. Zhao RL and He YM: Network pharmacology analysis of the anti-cancer pharmacological mechanisms of Ganoderma lucidum extract with experimental support using Hepa1-6-bearing C57 BL/6 mice. J Ethnopharmacol 210: 287-295, 2018.
23. Li ZH, Yu D, Huang NN, Wu JK, Du XW and Wang XJ: Immunoregulatory mechanism studies of ginseng leaves on lung cancer based on network pharmacology and molecular docking. Sci Rep 11: 18201, 2021.
24. Chen B, Liu C, Long H, Bai G, Zhu Y and Xu H: N^6-methyladenosine-induced long non-coding RNA PVT1 regulates the miR-27b-3p/BLM axis to promote prostate cancer progression. Int J Oncol 62: 16, 2023.
25. Safran M, Rosen N, Twik M, BarShir R, Stein TI, Dahary D, Fishilevich S and Lancet D: The GeneCards suite. In: Practical Guide to Life Science Databases. Abugessaisa I, Kasukawa T (editors). Springer Nature Singapore., Singapore, pp. 27-56, 2021.
26. Wishart DS, Feunang YD, Guo AC, Lo EJ, Marcu A, Grant JR, Sajed T, Johnson D, Li C, Sayeeda Z, *et al*: DrugBank 5.0: A major update to the DrugBank database for 2018. Nucleic Acids Res 46: D1074-D1082, 2018.
27. Hamosh A, Amberger JS, Bocchini C, Scott AF and Rasmussen SA: Online mendelian inheritance in man (OMIM®): Victor McKusick's magnum opus. Am J Med Genet A 185: 3259-3265, 2021.
28. Zhou Y, Zhang Y, Zhao D, Yu X, Shen X, Zhou Y, Wang S, Qiu Y, Chen Y and Zhu F: TTD: Therapeutic target database describing target druggability information. Nucleic Acids Res 52: D1465-D1477, 2024.
29. Huang DW, Sherman BT and Lempicki RA: Systematic and integrative analysis of large gene lists using DAVID bioinformatics resources. Nat Protoc 4: 44-57, 2009.
30. Huang DW, Sherman BT and Lempicki RA: Bioinformatics enrichment tools: Paths toward the comprehensive functional analysis of large gene lists. Nucleic Acids Res 37: 1-13, 2009.
31. Tianyu Z and Liying G: Identifying the molecular targets and mechanisms of xuebijing injection for the treatment of COVID-19 via network parmacology and molecular docking. Bioengineered 12: 2274-2287, 2021.
32. Livak KJ and Schmittgen TD: Analysis of relative gene expression data using real-time quantitative PCR and the 2(-Delta Delta C(T)) method. Methods 25: 402-408, 2001.
33. Chen P, Hsu WH, Han J, Xia Y and DePinho RA: Cancer stemness meets immunity: From mechanism to therapy. Cell Rep 34: 108597, 2021.
34. Sun SY: mTOR-targeted cancer therapy: Great target but disappointing clinical outcomes, why? Front Med 15: 221-231, 2021.
35. Song HP, Li RL, Zhou C, Cai X and Huang HY: Atractylodes macrocephala Koidz stimulates intestinal epithelial cell migration through a polyamine dependent mechanism. J Ethnopharmacol 159: 23-35, 2015.

36. Song HP, Hou XQ, Li RY, Yu R, Li X, Zhou SN, Huang HY, Cai X and Zhou C: Atractylenolide I stimulates intestinal epithelial repair through polyamine-mediated Ca(2+) signaling pathway. Phytomedicine 28: 27-35, 2017.
37. Liu M, Wang RB, Xing JH and Tang YX: Atractylenolide inhibits apoptosis and oxidative stress of HTR-8/SVneo cells by activating MAPK/ERK signalling in preeclampsia. Phytomedicine 93: 153773, 2021.
38. Du Z, Ma Z, Lai S, Ding Q, Hu Z, Yang W, Qian Q, Zhu L, Dou X and Li S: Atractylenolide I ameliorates acetaminophen-induced acute liver injury via the TLR4/MAPKs/NF-κB signaling pathways. Front Pharmacol 13: 797499, 2022.
39. Fan M, Gu X, Zhang W, Shen Q, Zhang R, Fang Q, Wang Y, Guo X, Zhang X and Liu X: Atractylenolide I ameliorates cancer cachexia through inhibiting biogenesis of IL-6 and tumour-derived extracellular vesicles. J Cachexia Sarcopenia Muscle 13: 2724-2739, 2022.
40. Waseh S and Lee JB: Advances in melanoma: Epidemiology, diagnosis, and prognosis. Front Med (Lausanne) 10: 1268479, 2023.
41. Kibbi N, Kluger H and Choi JN: Melanoma: Clinical presentations. Cancer Treat Res 167: 107-129, 2016.
42. Fu XQ, Chou JY, Li T, Zhu PL, Li JK, Yin CL, Su T, Guo H, Lee KW, Hossen MJ, *et al*: The JAK2/STAT3 pathway is involved in the anti-melanoma effects of atractylenolide I. Exp Dermatol 27: 201-204, 2018.
43. Castaneda M, den Hollander P, Kuburich NA, Rosen JM and Mani SA: Mechanisms of cancer metastasis. Semin Cancer Biol 87: 17-31, 2022.
44. Wei CY, Zhu MX, Yang YW, Zhang PF, Yang X, Peng R, Gao C, Lu JC, Wang L, Deng XY, *et al*: Downregulation of RNF128 activates Wnt/β-catenin signaling to induce cellular EMT and stemness via CD44 and CTTN ubiquitination in melanoma. J Hematol Oncol 12: 21, 2019.
45. Gong Q, Yu H, Ding G, Ma J, Wang Y and Cheng X: Suppression of stemness and enhancement of chemosensibility in the resistant melanoma were induced by Astragalus polysaccharide through PD-L1 downregulation. Eur J Pharmacol 916: 174726, 2022.
46. Kalluri R and Weinberg RA: The basics of epithelial-mesenchymal transition. J Clin Invest 119: 1420-1428, 2009.
47. Li B, Shen W, Peng H, Li Y, Chen F, Zheng L, Xu J and Jia L: Fibronectin 1 promotes melanoma proliferation and metastasis by inhibiting apoptosis and regulating EMT. Onco Targets Ther 12: 3207-3221, 2019.
48. Pan G, Liu Y, Shang L, Zhou F and Yang S: EMT-associated microRNAs and their roles in cancer stemness and drug resistance. Cancer Commun (Lond) 41: 199-217, 2021.
49. Battula VL, Evans KW, Hollier BG, Shi Y, Marini FC, Ayyanan A, Wang RY, Brisken C, Guerra R, Andreeff M and Mani SA: Epithelial-mesenchymal transition-derived cells exhibit multilineage differentiation potential similar to mesenchymal stem cells. Stem Cells 28: 1435-1445, 2010.
50. Qiao P and Tian Z: Atractylenolide I inhibits EMT and enhances the antitumor effect of cabozantinib in prostate cancer via targeting Hsp27. Front Oncol 12: 1084884, 2022.
51. Smalley KS: Understanding melanoma signaling networks as the basis for molecular targeted therapy. J Invest Dermatol 130: 28-37, 2010.
52. Wang Y, Chen SJ, Ma T, Long Q, Chen L, Xu KX and Cao Y: Promotion of apoptosis in melanoma cells by taxifolin through the PI3K/AKT signaling pathway: Screening of natural products using WGCNA and CMAP platforms. Int Immunopharmacol 138: 112517, 2024.
53. Sinnberg T, Lasithiotakis K, Niessner H, Schittek B, Flaherty KT, Kulms D, Maczey E, Campos M, Gogel J, Garbe C and Meier F: Inhibition of PI3K-AKT-mTOR signaling sensitizes melanoma cells to cisplatin and temozolomide. J Invest Dermatol 129: 1500-1515, 2009.
54. Yu R, Yu BX, Chen JF, Lv XY, Yan ZJ, Cheng Y and Ma Q: Anti-tumor effects of Atractylenolide I on bladder cancer cells. J Exp Clin Cancer Res 35: 40, 2016.
55. Wang J, Zhang P, Zhang J, Ma Z, Tian X, Liu Y, Lv G and Qu L: Atractylenolide-1 targets FLT3 to regulate PI3K/AKT/HIF1-α pathway to inhibit osteogenic differentiation of human valve interstitial cells. Front Pharmacol 13: 899775, 2022.
56. Akinleye A, Avvaru P, Furqan M, Song Y and Liu D: Phosphatidylinositol 3-kinase (PI3K) inhibitors as cancer therapeutics. J Hematol Oncol 6: 88, 2013.
57. Koyasu S: The role of PI3K in immune cells. Nat Immunol 4: 313-319, 2003.
58. Yan Y, Chou GX, Hui W, Chu JH, Fong WF and Yu ZL: Effects of sesquiterpenes isolated from largehead atractylodes rhizome on growth, migration, and differentiation of B16 melanoma cells. Integr Cancer Ther 10: 92-100, 2011.
59. Osaki M, Oshimura M and Ito H: PI3K-Akt pathway: Its functions and alterations in human cancer. Apoptosis 9: 667-676, 2004.
60. Liu Y, Jia Z, Dong L, Wang R and Qiu G: A randomized pilot study of atractylenolide I on gastric cancer cachexia patients. Evid Based Complement Alternat Med 5: 337-344, 2008.
61. Huang JM, Zhang GN, Shi Y, Zha X, Zhu Y, Wang MM, Lin Q, Wang W, Lu HY, Ma SQ, *et al*: Atractylenolide-I sensitizes human ovarian cancer cells to paclitaxel by blocking activation of TLR4/MyD88-dependent pathway. Sci Rep 4: 3840, 2014.